Acta Crystallographica Section B
Structural Science
ISSN 0108-7681

Electron density studies on hydrogen bonding in two chromone derivatives

Magdalena Małecka,[a]* Lilianna Chęcińska,[a] Agnieszka Rybarczyk-Pirek,[a] Wolfgang Morgenroth[b] and Carsten Paulmann[c,d]

[a]Department of Structural Chemistry and Crystallography, University of Łódź, Tamka 12, Poland, [b]Goethe Universität, Department of Geosciences, Altenhöferallee 1, D 60438 Frankfurt, Germany, [c]c/o DESY/HASYLAB, Notkestrasse 85, 22603 Hamburg, Germany, and [d]Mineralogisch-Petrographisches Institut, Universität Hamburg, Grindelallee 48, D 20146 Hamburg, Germany

Correspondence e-mail: malecka@uni.lodz.pl

Received 16 June 2010
Accepted 12 October 2010

The experimental electron densities of two chromone derivatives have been determined from X-ray synchrotron diffraction data at low temperature (100 K). Topological analysis of the electron density has been used to analyze the formation of resonance-assisted hydrogen bonds (RAHBs). Geometrical and topological parameters confirm π-electron delocalization within the hydrogen-bonded ring. In addition, weak C—H···O interactions were identified in both structures. Hydrogen-bond energies allowed medium and weak hydrogen bonds to be distinguished.

1. Introduction

Ultra-high-resolution X-ray charge density experiments provide information on the precise electron density distribution (EDD) as a helpful tool for characterizing the electronic properties of bonding and non-bonding interactions (Koritsanszky & Coppens, 2001). Bader's approach of 'Atoms in Molecules' (AIM; Bader, 1990) allows a topological analysis of $\rho(\mathbf{r})$, yielding a quantitative description of atoms, bonds and non-bonding interactions. Experimental EDD can be derived using the Hansen–Coppens multipolar atom model (Hansen & Coppens, 1978), which is used in the multipole refinement of high-resolution X-ray diffraction data.

In this paper experimental methods were applied to derive a charge density distribution for two chromone derivatives. Bader's AIM approach was used to analyze the experimental EDD as part of ongoing investigations. Research on chromone and coumarin derivatives has been stimulated by their promising pharmacological, analytical and agrochemical applications (Rosskopt *et al.*, 1992; Ohemeng *et al.*, 1993; Kostova, 2007; Musa *et al.*, 2008). Alkylating properties of these compounds have been extensively investigated and widely described in many papers (Budzisz *et al.*, 2002, 2003; Kulkarni *et al.*, 2006; Przybylski *et al.*, 2009; Asmah Susidarti *et al.*, 2009). Owing to their ability to coordinate metal ions, transition metal complexes with chromone as well as coumarin derivatives show significant biological activity and they are the subject of current research (Grazul & Budzisz, 2009).

The experimental charge densities of 3-(aminophenylmethylene)chroman-2,4-dione (I) and the compound 3-(methylaminophenylmethylene)chroman-2,4-dione (II) [see (I) and Fig. 1] were determined. Our main interest is in the intramolecular hydrogen bond which closes an extra six-membered hydrogen-bonded ring and is common to both compounds. Homonuclear resonance-assisted hydrogen bonds (RAHBs) have been subjected to a charge density study before (Madsen *et al.*, 1998). With respect to the geometrical parameters within this heteronuclear O=C—C=C—N—H keto-amine ring the N—H···O interaction can be classified as

© 2010 International Union of Crystallography
Printed in Singapore – all rights reserved

a RAHB. RAHBs are present in many biological systems taking part in various biochemical processes and are therefore an important factor in biochemistry and molecular biology (Jeffrey, 1997; Jeffrey & Saenger, 1991). The concept of RAHBs was proposed by Gilli on the basis of keto–enol tautomerism (Gilli *et al.*, 1989) for O—H···O homonuclear hydrogen bonds. In this and later studies it was pointed out that the phenomenon of RAHBs may be described by the contribution of two tautomeric forms connected *via* proton transfer: O/N—H···O ↔ O/N···H—O for homonuclear and heteronuclear systems. It was stated that for RAHBs a π-electron delocalization within the O=C—C=C—O/N—H keto–enol/amine hydrogen-bonded ring has been observed.

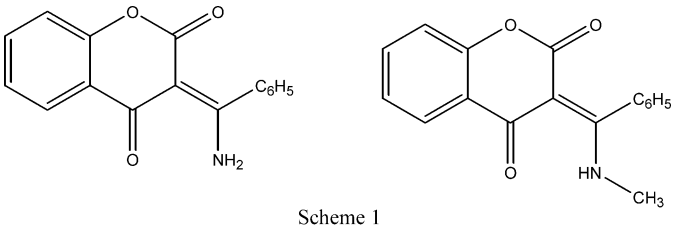

Scheme 1

The chromone and coumarin derivatives, as well as oxaphosphinane ones which also contain a RAHB system, were systematically examined experimentally and theoretically (Małecka, 2007; Małecka *et al.*, 2004; Grabowski & Małecka, 2006; Rybarczyk-Pirek *et al.*, 2002, 2006).

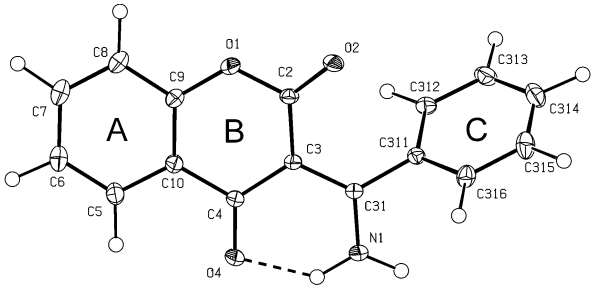

(*a*)

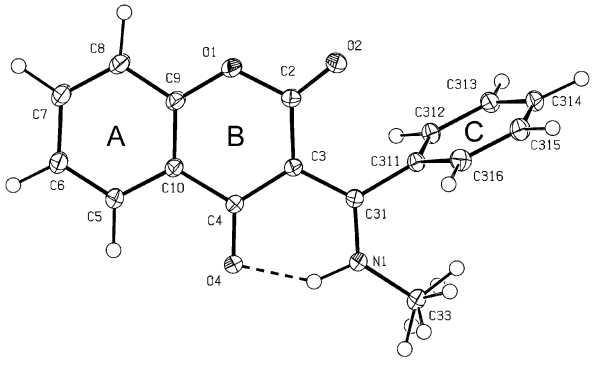

(*b*)

Figure 1
Molecular structure with atom-numbering scheme of (*a*) (I) and (*b*) (II) showing the displacement ellipsoids at the 50% probability level. The intramolecular N—H···O hydrogen bonds are displayed as dashed lines. *ORTEP* (Burnett & Johnson, 1996) representation: H atoms are drawn as small spheres of arbitrary radii.

It is worth mentioning that the concept of RAHB has been criticized recently (Alkorta *et al.*, 2004, 2005). The authors explain that the increased strength of hydrogen bonds for RAHB systems is associated with the σ-skeleton of the molecule, which allows the donor and acceptor atoms to be closer in unsaturated systems than in the corresponding saturated compounds. On the other hand, 20–30% of the hydrogen-bond energy is connected with the π-electron delocalization and 70–80% with the energy attributed to closer proximity of the donor and acceptor atom (Grabowski, 2003). Discussions on the RAHB concept raise the question that if a π-electron delocalization exists in the hydrogen-bonded ring of the investigated systems, can any characteristic features of these systems, such as geometrical or topological parameters, confirm the existence of RAHBs? In our opinion the study of the experimental electron density distribution within the six-membered rings helps to answer these questions.

2. Experimental procedures and structure determination

Single crystals suitable for charge density analysis were obtained by recrystallization of the compounds by slow evaporation from ethanol solution. Since crystals of (II) were too big they were partly dissolved in a mixture of ethanol and heptane until they were shaped like spheres with a diameter of ~ 0.55 mm. For (I) a crystal of $0.35 \times 0.28 \times 0.20$ mm was used.

High-resolution X-ray diffraction data were collected at beamline F1 of the storage ring DORIS III at HASYLAB/DESY, Hamburg, Germany. Beamline F1 is equipped with a kappa-axis four-circle Huber diffractometer and a MAR165 CCD detector. The temperature for the experiment was maintained at 100 K with an Oxford Cryosystem N_2 gas-stream cooling device. For (I) four shells of reciprocal space were covered with the CCD detector by 1° φ rotations with goniometer setting angles 2θ, ω, χ, positioned at 0, 0, 0; −45, 0, 0; and −45, 0, 60°. Exposure times of 5 and 10 s for runs at 2θ = 0° and 90 s for high 2θ setting runs were chosen. Using these settings 200 890 reflections were collected within ∼29 h up to a resolution of $\sin\theta/\lambda = 1.12$ Å^{-1}. For (II) two 'zero' runs with exposure times of 5 and 10 s and three 'high'-order runs with angle settings of 2θ, ω, χ: −45, 0, 0; −55, −30, 60; −55, 20, 60° and a scan time of 90 s were measured. This setting gave 117 495 collected reflections up to a resolution of $\sin\theta/\lambda$ = 1.18 Å^{-1} for (II). The integration, data reduction and scaling of diffracted intensities were carried out using the *XDS* package, version 2009 (Kabsch, 1993). At this point intensities were corrected for the oblique incidence of X-rays on the detector surface [Johnas *et al.*, 2006; Paulmann, 2006, for (I) and (II)]. The data for (I) were converted using the *d3_reduce* program (Overgaard & Madsen, 2007) and merged with the *SORTAV* program. 846 outliers were removed. The remaining reflections were merged to give 14 726 unique reflections (with an average redundancy of 13.6) and an internal agreement factor of 3.61%. Merging for the second set of intensities [for

Table 1
Crystal data and structure refinement for (I) and (II).

Experiments were carried out at 100 K with synchrotron radiation, λ = 0.6000 Å using a Huber diffractometer. Refinement was with 0 restraints.

	(I)	(II)
Crystal data		
Chemical formula	$C_{16}H_{11}NO_3$	$C_{17}H_{13}NO_3$
M_r	265.26	279.28
Crystal system, space group	Orthorhombic, *Pbca*	Monoclinic, $P2_1/c$
a, *b*, *c* (Å)	12.925 (3), 8.273 (2), 23.954 (5)	9.292 (2), 14.145 (2), 11.012 (2)
β (°)	90	110.576 (3)
V (Å^3)	2561.4 (9)	1355.0 (4)
Z	8	4
μ (mm^{-1})	0.10	0.10
Crystal size (mm)	0.35 × 0.28 × 0.20	0.55 × 0.5 × 0.45
Data collection		
sin θ/λ (Å^{-1})	1.12	1.18
Completeness to sin θ/λ (%)	99.9	96.6
No. of measured, independent and observed [$I > 2\sigma(I)$] reflections	200 890, 14 726, 12 633	117 495, 17 962, 16 349
R_{int}	0.036	0.023
Redundancy	13.6	6.5
Spherical atom refinement		
Data/restraints/parameters	14 726/0/227	17 530/0/231
Goodness-of-fit on F^2	1.041	1.072
Final *R* indices [$I > 2\sigma(I)$]	R_1 = 0.0361, wR_2 = 0.1164	R_1 = 0.0324, wR_2 = 0.0910
Final *R* indices (all data)	R_1 = 0.0421, wR_2 = 0.1215	R_1 = 0.0346, wR_2 = 0.0929
Multipole atom refinement		
No. of data	14 158	17 530
No. of reflections	12 657	16 349
No. of parameters	438	464
N_{ref}/N_v	28.9	35.2
$\Delta\rho_{max}$, ρ_{min} (e Å^{-3})	0.207, −0.217	0.221, −0.231
Final $R_1(F)$	0.025	0.025
Final $R_{1\ all}(F)$	0.029	0.027
Final $wR_2(F)$	0.024	0.026
Goodness-of-fit	2.27	2.98

Computer program used: *MarCCD* (Paulmann, 2006), *XDS* (Kabsch, 1993), *SHELXS*97 (Sheldrick, 2008), *XD* (Volkov *et al.*, 2006)

(II)] was performed with *XPREP*; 4931 reflections were discarded and the remaining reflections were averaged to give 17 962 unique reflections with an average redundancy of 6.5.

The structures were solved using *SHELXS*97 (Sheldrick, 2008) and an initial refinement of the X-ray structure was carried out using *SHELXL*97 (Sheldrick, 2008). During the refinement of (II) the H atoms of the methyl group were found to be disordered over two positions, therefore occupancies were kept in the multipole refinement at 50%. Refinement of isotropic displacement parameters of the disordered atoms was not performed and they were assigned U_{iso} values of 1.5 times the U_{iso} value of the C atom they are attached to.

3. Aspherical atom model

The Hansen and Coppens multipole formalism (Hansen & Coppens, 1978) was used as implemented in the *XD* program package (Volkov *et al.*, 2006). The multipolar expansion of the electron density distribution, as expressed with $\rho_c(r)$ and $\rho_v(\kappa r)$ representing the spherical core and valence electron densities, is composed of Hartree–Fock wavefunctions expanded by Slater-type basis functions (Clementi & Roetti, 1974) and is contractable/expandable by the κ parameter. For the deformation terms single zeta orbitals with energy-optimized Slater exponents were taken and kept fixed. The multipole refinements were carried out with the full-matrix least-squares refinement program (*XDLSM*) of the *XD* program package. The quantity $\sum_{\mathbf{h}} w_{\mathbf{h}} |F_{obs}(\mathbf{h}) - kF_{calc}(\mathbf{h})|^2$ was minimized using the statistical weight $w_{\mathbf{h}} = 1/\sigma^2(F^2(\mathbf{h}))$ and only those structure factors that matched the criterion of $F^2_{obs}(\mathbf{h}) > 2\sigma(F^2_{obs}(\mathbf{h}))$ were included.

3.1. Refinement of the multipole model

The starting positional and displacement parameters for the non-H atoms were taken from the spherical atom refinement and re-refined with high-angle reflections (sin θ/λ ≥ 1.0 Å^{-1}). These parameters were kept fixed in the subsequent independent atom model (IAM) refinement steps. H atoms were then re-refined using the low-order data (sin θ/λ < 0.5 Å^{-1}). The methyl H atoms in (II) were refined as a rigid group of disordered H atoms with occupancies of 0.5. The multipole model refinement was carried out as follows: for non-H atoms positional, displacement and multipole parameters up to the hexadecapole level were refined, whereas for H atoms they were refined up to the dipolar level. The C—H and N—H bonds were elongated to standard values from neutron diffraction (Allen *et al.*, 1992) after the initial monopole refinement. The C—H bonds within the disordered methyl group were also elongated, the position of H atoms was not refined and U_{iso} values were fixed. In order to reduce the numbers of variables, atomic site-symmetry conditions were applied by fixing the $P_{lm\pm}$ parameters to zero according to the selection rules for spherical harmonics. During the multipole refinement the following constraints were used: for (I) local mirror C_s symmetry was imposed on all C, N and O atoms, C5 was constrained to C8, C6 to C7, C312 to C316 and C313 to C315. Furthermore, H6, H7, H8 were constrained to H5, and similarly H313, H314, H315, H316 were constrained to H312. For (II) local mirror C_s symmetry was imposed for all C, N and O atoms excluding C31 without symmetry restriction, and for the C33 atom a local C_3

symmetry was included. H atoms were treated as in (I). After refinement at the hexadecapolar level the κ parameters were refined independently for non-H atoms. In the next step H-ADPs (atomic displacement parameters) were generated by the *SHADE* program (Madsen, 2006). Finally, all the multipole parameters were refined with fixed ADPs for H atoms. The correctness of these restrictions was assessed with respect to convergence, residual density and topological parameters in comparison to a model free of symmetry. Further details of the multipole models for (I) and (II), which are referred to as *Mul_exp_I* and *Mul_exp_II*, are presented in Table 1. The residual density maps in Fig. S1 of the supplementary material[1] are featureless, indicating an adequate description of the experimental data by the multipole models. The module XDPROP of the package *XD* was used for the topological analysis of the electron densities. The source function calculations on the experimental models used the keywords SOURCE and TOPINT.

3.2. Theoretical model

The single-point and gas-phase theoretical calculations based on experimental geometry were performed with density functional theory (DFT) using the program package *GAUSSIAN*03 (Frisch *et al.*, 2003) with the B3LYP functional (Becke, 1993) and the standard basis set 6-311++G**. A topological analysis was performed with the program *AIM*2000 (Biegler-König & Schonbohm, 2002). Values resulting from these calculations are referred to model *SP_theo* (single-point calculation) and *OPT_theo* (geometry optimization in the gas phase).

4. Results

4.1. Description of the crystal structure

The molecular structures of (I) and (II) are displayed in Fig. 1 as an *ORTEP* (Burnett & Johnson, 1996) representation including the labelling scheme. The examined molecules (I) and (II) consist of the chroman-2,4-dione system (rings *A*, *B*) substituted by different groups: phenyl-ethylamine (I) and methyl-phenyl-ethylamine (II) at position 3. A comparison of the geometric experimental data for both molecules shows an average difference of corresponding bond lengths and angles of 0.01 Å and 0.4° (Table S1). The only exception is the C31—N1—H1 angle, with the difference is 5.7°. It seems that the presence of the methyl group might cause this difference. Additionally, considering the angle between the *AB* ring system and the *C* ring, a larger dihedral angle of 73.4° is observed in (II) with respect to a corresponding value of 53.2° for (I). This effect might be caused by steric repulsion between methyl and phenyl groups forced by methyl substitution. The selected bonds and angles in the main part of the chromone moiety compared with the corresponding values of previously examined chromone derivatives (Małecka *et al.*, 2004; Małecka & Budzisz, 2006) do not differ significantly. There are some exceptions to the N—H distances as a consequence of the different treatment of H atoms during the refinement procedure (in some cases the AFIX procedure was applied in *SHELXL*97; Sheldrick, 2008).

The crystal structures of (I) and (II) reveal the existence of intramolecular N—H···O hydrogen bonds, which close extra six-membered rings. These interactions can be classified as resonance-assisted hydrogen bonds (RAHBs). Similarly RAHBs were analyzed previously for other chromone and oxaphosphinane derivatives (Małecka, 2007; Małecka & Budzisz, 2006). The geometrical and energetical consequences of a RAHB hydrogen-bond formation will be discussed in detail in §4.2.

Fig. 2 shows the crystal packing of (I) and (II). The intermolecular hydrogen bonds in molecule (I) are arranged in three chains with zigzag shape. The N1—H1···O2^{i} hydrogen bond leads to an infinite chain along the *b* axis described by the graph-set motif *C*(6) (Etter, 1990; Bernstein *et al.*, 1995). Similarly, the C312—H312···O2^{ii} intermolecular interaction results in a zigzag arrangement of molecules and gives the chain *C*(7) along the *b* axis. The third interaction C7—H7···O4^{iii} forms an infinite *C*(7) chain parallel to the *a* axis. The combination of chains generates a single continuous

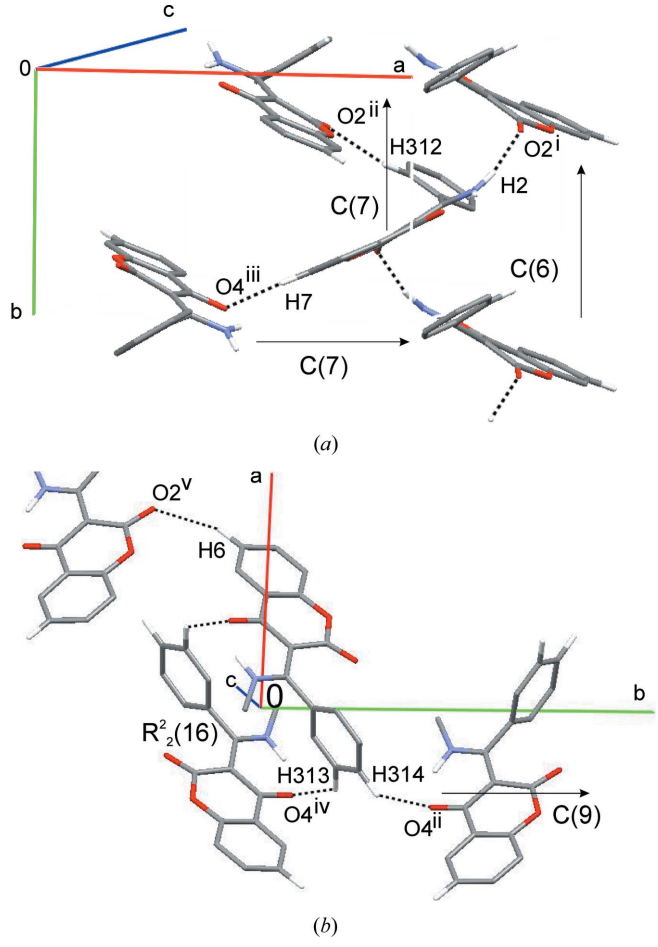

Figure 2
Hydrogen-bond network in the unit cell: (*a*) (I) and (*b*) (II).

[1] Supplementary data for this paper are available from the IUCr electronic archives (Reference: SN5099). Services for accessing these data are described at the back of the journal.

Table 2
Geometrical (in Å, °) and topological parameters for intra- and intermolecular hydrogen bonds (ρ in e Å^{-3}, $\nabla^2\rho$ in e Å^{-5}).

For the intramolecular N1—H1···O4 hydrogen bond the first line refers to the *Mul* model, the second to *SP_theo* and the third to *OPT_theo*.

	D—H	H···*A*	*D*···*A*	*D*—H···*A*	ρ	$\nabla^2\rho$
(I)						
N1—H1···O4	1.01	1.82	2.596 (1)	131	0.30 (2)	3.4 (1)
	1.01	1.82	2.597	131	0.25	3.3
	1.02	1.75	2.576	134	0.29	3.5
N1—H2···O2^{i}	1.01	1.89	2.879 (1)	164	0.17 (2)	2.6 (1)
C312—H312···O2^{ii}	1.08	2.32	3.227 (1)	140	0.07 (1)	1.1 (1)
C7—H7···O4^{iii}	1.08	2.34	3.419 (1)	177	0.06 (1)	1.0 (1)
(II)						
N1—H1···O4	1.01	1.70	2.596 (1)	145	0.32 (1)	4.6 (1)
	1.01	1.71	2.596	145	0.30	3.6
	1.03	1.69	2.569	141	0.35	3.8
C313—H313···O4^{iv}	1.08	2.56	3.332 (1)	128	0.05 (1)	0.7 (1)
C6—H6···O2^{v}	1.08	2.52	3.512 (1)	152	0.04 (3)	0.7 (1)
C314—H314···O4^{ii}	1.08	2.32	3.188 (1)	136	0.07 (1)	1.1 (1)

Symmetry code: (i) $1-x, -\frac{1}{2}+y, \frac{1}{2}-z$; (ii) $\frac{1}{2}+x, \frac{1}{2}-y, -z$; (iii) $\frac{3}{2}-x, -\frac{1}{2}+y, z$; (iv) $-x, \frac{1}{2}+y, -\frac{1}{2}-z$; (v) $-x, -y, -z$.

Table 3
Geometrical (Å, °) and topological parameters for bonds within the hydrogen-bonded ring for the resonance-assisted hydrogen bond (ρ in e Å^{-3}, $\nabla^2\rho$ in e Å^{-5}).

The first line refers to model *Mul*, the second to *SP_theo* and the third one to *OPT_theo*.

	d	ρ	∇^2	ϵ
(I)				
O4—C4, *d*1	1.2562 (4)	2.42 (2)	−16.2 (1)	0.10
	1.2562	2.52	−8.9	0.03
	1.2446	2.57	−7.1	0.03
C3—C4, *d*2	1.4526 (3)	1.82 (2)	−10.9 (1)	0.19
	1.4526	1.90	−17.3	0.19
	1.4589	1.88	−16.9	0.18
C3—C3, *d*3	1.4327 (4)	1.87 (1)	−12.8 (1)	0.21
	1.4327	1.93	−17.5	0.21
	1.4109	2.01	−19.1	0.25
N1—C31, *d*4	1.3216 (4)	2.24 (2)	−18.6 (1)	0.17
	1.3216	2.30	−20.5	0.15
	1.3333	2.26	−21.4	0.12
N1—H1	1.0090	2.02 (2)	−16.4	–
	1.0090	2.27	−45.8	–
	1.0265	2.17	−41.8	–
(II)				
O4—C4, *d*1	1.2569 (2)	2.58 (2)	−15.7 (1)	0.10
	1.2570	2.51	−8.9	0.03
	1.2488	2.55	−7.5	0.03
C3—C4, *d*2	1.4469 (2)	1.83 (2)	−10.6 (1)	0.18
	1.4469	1.92	−17.6	0.19
	1.4540	1.89	−17.1	0.19
C3—C31, *d*3	1.4301 (2)	1.86 (2)	−12.9 (1)	0.19
	1.4301	1.93	−17.7	0.24
	1.4210	1.97	−18.4	0.25
N1—C31, *d*4	1.3258 (2)	2.27 (2)	−17.9 (1)	0.21
	1.3258	2.29	−20.7	0.12
	1.3292	2.27	−20.7	0.12
N1—H1	1.0088	2.21 (2)	−22.1 (1)	–
	1.0090	2.29	−46.3	–
	1.0282	2.15	−40.8	–

three-dimensional framework structure. The aromatic rings are in close contact, showing π–π stacking interactions between rings *B* and *C*. The distance between the ring centroids Cg(*B*)···Cg(*C*) $(1-x, \frac{1}{2}+y, \frac{1}{2}-z)$ is 3.669 (1) Å. The molecules of (II) are linked to the centrosymmetric ring $R_2^2(16)$ by two C313—H313···O4^{iv} hydrogen bonds. Each molecule of the ring is involved as part of two independent chains, *C*(8) and *C*(9), parallel to the *b* axis. The chains are generated by the corresponding C6—H6···O2^{v} and C314—H314···O4^{ii} hydrogen bonds. Compound (II) also contains intermolecular C—H···π contacts, where C7—H7 interacts with the C phenyl ring related by symmetry $1+x, y, 1+z$. The C7···Cg(C) distance is 3.698 (1) Å, H7···Cg(C) is 2.71 Å, while the C7—H7···Cg(C) angle equals 152°. Table 2 shows the geometric details of the previously mentioned hydrogen interactions.

4.2. Hydrogen bonds

4.2.1. RAHBs and their structural and topological consequences. The most characteristic feature for RAHBs of heteronuclear systems (Scheme 2; Bertolasi *et al.*, 1994) is that they result in two general changes of the corresponding geometrical parameters (Scheme 2):

(i) equalization of the lengths of the bonds d_2 and d_3,

(ii) shortening of the C—N bond and lengthening of C═O bonds for heteronuclear systems with respect to other corresponding bonds not involved in hydrogen-bond interaction.

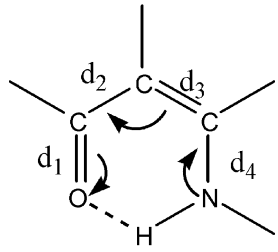

Scheme 2

According to the structural changes, the delocalization of π-electrons is observed within the hydrogen-bond motif (O═C—C═C—N—H) containing conjugated formal single and double bonds.

As can be observed in Table 3 the formally single bond (d_2) appears shorter and the double one (d_3) appears longer than the reference values (Allen *et al.*, 1987). The average bond distance for the formally single d_2 bond is 1.4495 Å, while the average bond distance d_3 (the formally double one) is 1.4314 Å. This is in agreement with our previous results (Małecka & Budzisz, 2006). For these systems the d_2 distance is in the range 1.430–1.445 Å (with an average value of 1.438 Å) and d_3 is in the range 1.412–1.438 Å (with an average value of 1.423 Å). It is worth noting that according to Allen (Allen *et al.*, 1987) the formal single C3—C4 and double C3═C31 bonds in such systems are 1.464 and 1.340 Å. Further

comparison can be made for C4═O4 (d_1) and C31—N1 (d_4) within the additional closed ring. A lengthening is observed in the C4═O4 bond (d_1) and a shortening of the C—N (d_4) bond with respect to the expected values for structures in which the N atom is not involved in a hydrogen bond (Allen *et al.*, 1987). This observation leads to the conclusion that π-electron delocalization within a O═C—C═C—N—H conjugated bond system exists and is further strengthened owing to the intramolecular RAHB formation.

Topological parameters obtained using Bader's AIM approach may also give a quantitative description about the π-electron distribution within the hydrogen-bonded ring. Experimental electron densities of the intramolecular hydrogen bonds are illustrated qualitatively in the static deformation maps presented in Fig. 3. The electron densities of the C3—C4 and C3—C31 bonds (see Table 3) do not differ significantly; $\rho_{exp}(\mathbf{r})$ for (I): 1.82 (1) and 1.87 (1) e Å^{-3}; for (II): 1.83 (2) and 1.86 (2) e Å^{-3}. It shows nearly equal values within 3σ criteria. The average $\rho_{exp}(\mathbf{r})$ values of aromatic bonds (C_{ar}—C_{ar}) in the phenyl rings (C) are 1.90 (2) and 1.92 (2) e Å^{-3} for (I) and (II), close to the values presented above. Moreover, the electron density values for C3—C4 and C3—C31 bonds of analyzed rings (as mentioned above) are higher than the electron density of the formal C31—C311 single bond [1.70 (2) and 1.68 (2) e Å^{-3} for (I) and (II)]. These results indicate that there is no π-electron communication between the RAHB system and the phenyl ring, while such communication is observed between the hydrogen-bonded ring and the aromatic *A* ring. The values of $\rho_{exp}(\mathbf{r})$ for C31—N1 and C4═O4 bonds are also comparable for both compounds. However, the electron density of both C4═O4 bonds is distinctly weaker than for C2═O2 bonds [$\rho_{exp}(\mathbf{r})$ C2═O2 is 2.80 (2) and 2.87 (2) e Å^{-3}, for (I) and (II)]. These results also confirm a π-electron delocalization within a hydrogen-bonded ring containing a conjugated systems of single and double bonds.

Comparing theoretical and experimental topological descriptors within the RAHB system good agreement between experiment and theory is observed. For C—C bonds agreement between the *Mul_exp*, *SP_theo* and *OPT_theo* models is within 0.1–0.2 e Å^{-3} and 2–6 e Å^{-5} for $\rho(\mathbf{r})$ and $\nabla^2\rho(\mathbf{r})$, while the differences for C—N bonds are within 0.02–0.06 e Å^{-3} and 1–3 e Å^{-5} $\rho(\mathbf{r})$ and $\nabla^2\rho(\mathbf{r})$. The largest discrepancies are observed for C═O bonds. A similar observation of results has been explained in the literature as being a consequence of the limited flexibility of radial functions in the multipole model (Gatti *et al.*, 1992; Volkov *et al.*, 2000; Bach *et al.*, 2001). Furthermore, C═O and N—H bonds represent regions where the intermolecular interactions are not considered (in theoretical calculations), whereas they occur in the crystal lattice.

The π-character of a bond can be revealed by the bond ellipticity ϵ, which describes the asymmetry of the electron distribution between two bonded atoms. The ellipticity is defined by $\epsilon = \lambda_1/\lambda_2 - 1$ as a measure of the anisotropy of the curvature of the electron density in directions normal to the bond. It is related to λ_1 and λ_2, the eigenvalues of the Hessian of the electron density $\rho(\mathbf{r})$.

While for the nonpolar bonds ϵ provides a rather sensitive measure of the degree of π delocalization, the interpretation becomes more difficult in the case of heteropolar bonds like C—N. Pure single, double and triple C—C bonds have ellipticity values ϵ equal to 0.014, 0.298 and 0.000 in butane, ethene and ethyne (Popelier, 2000). The π-delocalization within the hydrogen-bonded ring is correctly reflected in the ellipticity/topology of the static electron density model. Ellipticity values for the hydrogen-bonded ring fragments range from 0.1 to 0.21. Thus, ellipticities for the C3—C31 and the C3—C4 bonds are close to the ellipticities in the benzene ring. The average ellipticity values in aromatic benzene rings is 0.20. The model of RAHB also predicts π-delocalization in the C═O and C—N bonds. As seen in Table 3, the experimental values of the ellipticities suggest the presence of a delocalized π-system in the whole keto-amine group. It is worth noting that the ellipticity for formal single and double C—C bonds does not differ by more than 0.02. The large values of the ellipticity allow all bonds to be characterized within the investigated O═C—C═C—N—H ring as having partial π-character. The comparison of bond distances, electron density $\rho(\mathbf{r})$ and ellipticity ϵ indicates that π-delocalization exists within the hydrogen-bonded ring.

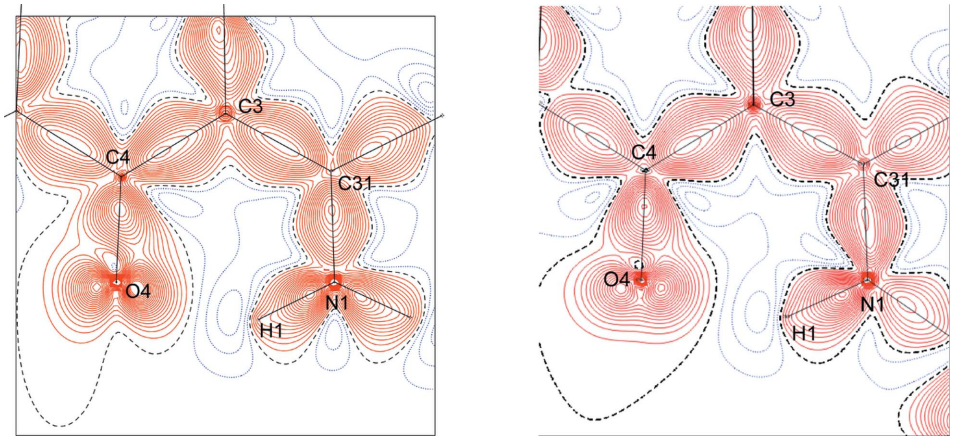

Figure 3
Static deformation density map for the extra six-membered ring of (*a*) (I) and (*b*) (II). Positive, zero and negative lines are in red, black and blue; the contour intervals are 0.05 e Å^{-3}.

4.2.2. Topological parameters for hydrogen bonds. Both chromone derivatives take part in intramolecular hydrogen bonds, in one case N—H···O intermolecular hydrogen bonds and a few weaker intermolecular C—H···O contacts in the crystal structure.

Table 4
Hydrogen-bonding energies (in kJ mol^{-1}) and local energy densities (in kJ mol^{-1} per atomic unit volume).

E_{HB} geom calculated according to Espinosa *et al.* (1998); $E = 25.5 \times 10^3 e^{-3.6(H\cdots A)}$) and $E_{HB} = \frac{1}{2}V(\mathbf{r}_{BCP})$. For the intramolecular N1—H1···O4 hydrogen bond the first line refers to the *Mul* model, the second to *SP_theo* and the third to *OPT_theo*.

	E_{HB} geom	E_{HB}	G	V	H
(I)					
N1—H1···O4	−36.10	−56.53	102.75	−113.06	−10.31
	−35.74	−43.01	86.03	−88.94	−2.91
	−45.98	−52.93	100.93	−105.87	−4.94
N1—H2···O2^{i}	−28.07	−27.89	64.01	−55.77	8.24
C312—H312···O2^{ii}	−5.97	−9.16	24.67	−18.32	6.35
C7—H7···O4^{iii}	−5.55	−7.30	21.06	−14.61	6.45
(II)					
N1—H1···O4	−55.62	−68.59	131.67	−137.18	−5.51
	−48.07	−55.53	104.39	−111.06	−6.67
	−58.65	−66.18	117.69	−132.37	−14.67
C313—H313···O4^{iv}	−2.52	−4.88	13.99	−9.77	4.23
C6—H6···O2^{v}	−2.90	−4.53	13.72	−9.06	4.66
C314—H314···O4^{ii}	−5.97	−9.05	24.23	−18.10	6.13

Symmetry codes: (i) $1-x, -\frac{1}{2}+y, \frac{1}{2}-z$; (ii) $\frac{1}{2}+x, \frac{1}{2}-y, -z$; (iii) $\frac{3}{2}-x, -\frac{1}{2}+y, z$; (iv) $-x, \frac{1}{2}+y, -\frac{1}{2}-z$; (v) $-x, -y, -z$.

Table 5
Source contributions at the BCPs of the N1—H1···O4 hydrogen bond (ρ in e Å^{-3}).

	ρ	$S(H)$%	$S(D)$%	$S(A)$%	$S(H+A)$%	$S(H+D)$%
(I)						
N1—H1···O4	0.30 (2)	5.9	22.5	19.6	25.6	28.4
(II)						
N1—H1···O4	0.32 (1)	1.4	27.8	21.8	23.3	29.3

The AIM approach can also be used to characterize hydrogen bonding. There are eight topological parameters defining the existence and type of hydrogen bond (Koch & Popelier, 1995). With respect to these criteria all C—H···O interactions in the discussed crystal structures are weak. The strongest contact, C312—H312···O2^{iii}, has the highest electron density, $\rho(\mathbf{r}) = 0.07\ (1)$ e Å^{-3}, and the shortest H···O contact of 2.32 Å. These findings can be compared with the hydrogen-bond energy obtained from the distance-dependent relation $E = 25.3 \times 10^3 e^{-3.6(H\cdots A)}$ kJ mol^{-1} (Espinosa *et al.*, 1998), as given in Table 4. The other topological parameters are also listed in Table 4. The local kinetic energy density $G(\mathbf{r}_{BCP})$ has been derived from the electron density $\rho(\mathbf{r})$ and its Laplacian $\nabla^2\rho(\mathbf{r})$ *via* the Abramov expression (Abramov, 1997). Additionally, the total energy density $H(\mathbf{r}_{BCP})$ was used to classify the hydrogen-bonding type (Espinosa *et al.*, 2002). Based on the potential electron energy density the hydrogen-bond energy could also be estimated following Espinosa (Espinosa *et al.*, 1998), $E_{HB} = \frac{1}{2}V(\mathbf{r}_{BCP})$. Estimated binding energies are comparable with those calculated from distance-dependent relations. Taking into account both $H(\mathbf{r}_{BCP})$ and $\nabla^2\rho(\mathbf{r}_{BCP})$ we can classify the character of the interactions compared with the strength of the hydrogen bond (Rozas *et al.*, 2000). According to this approach the intramolecular N1—H1···O4 hydrogen bond shows a partially covalent character in both structures. Additionally, the energy value of the hydrogen bonds indicates that both intramolecular N—H···O hydrogen bonds are of medium strength. It is important to note that experimental values for the hydrogen-bond energy and G, H, V values are consistent with theoretical ones for the single-point calculation and the optimized geometry.

4.2.3. The source function in the RAHB system. The nature of a hydrogen bond can also be revealed by the source function introduced by Gatti & Bader (1998). The source function is found to be a sensitive measure for the nature of a hydrogen bond. This concept is based on the fact that the value of the electron density at any point in space may be separated into a sum of atomic contributions from every atom within the molecule. For RAHBs the source contribution from hydrogen appears positive but close to zero. It is slightly negative for polarized assisted hydrogen bonds, highly negative for isolated hydrogen bonds and largely positive for charge-assisted hydrogen bonds (Gatti *et al.*, 2003). The computed values are listed in Table 5. A positive contribution is observed for the H1···O4 interaction in both compounds. Furthermore, the contribution of donor and acceptor atoms is also positive and comparable. This finding is in accordance with the above-mentioned results and classifies the H1···O4 hydrogen bond as a resonance-assisted hydrogen bond.

Table 6
Summary of experimental atomic volumes V_{tot}, V_{001} in Å^3, number of electrons N, N_{001} in e and net atomic charges Q in e.

	(I)			(II)		
Atom	V_{tot}	V_{001}	Q	V_{tot}	V_{001}	Q
O1	15.86	15.03	−0.94	17.17	14.55	−0.81
O2	16.71	15.78	−0.88	19.44	17.16	−0.75
O4	16.69	15.71	−0.82	15.39	14.07	−0.68
N1	17.93	16.69	−1.10	12.23	11.96	−0.86
C2	6.72	6.49	1.13	9.21	7.62	1.02
C3	10.95	10.68	−0.14	10.97	10.54	−0.07
C4	8.15	7.35	0.66	7.27	7.26	0.53
C31	9.35	8.70	0.25	8.60	8.50	0.29
H1	3.60	3.08	0.43	3.11	3.12	0.29

5. Atomic properties

To evaluate atomic volumes and charges the module TOPXD of the *XD* package was used. The numerical results of the data integration for selected atoms of both compounds are summarized in Table 6 (Table S2 contains data integration results for all atoms). The quantity with index 'tot' is defined for volumes within interatomic boundaries in the crystal, while '001' is based on a cut-off of $\rho = 0.001$ a.u. (atomic units). Since the charge density in the outer regions of an atomic basin does not contribute substantially to its charge, the net atomic charges Q_{tot} and Q_{001} are in most cases practically equal, so that only one charge column Q_{tot} is given.

Bader atomic volumes and charges are additive. Therefore, the sum of the atomic volumes in one unit cell should be equal

to the experimental cell volume. For both compounds the sum of V_{tot} (multiplied by Z = 8/4) reproduces the unit-cell volumes within 1%. Similarly, the sum of the atomic charges should add up to zero. The charges differ by 0.01 e from electroneutrality for (I) and (II) – a negligible amount. For the N1 atom substituted by CH_3 (II) a slightly smaller volume (12.23 Å^3) with respect to the unsubstituted N1 atom in (I) (15.93 Å^3) is observed. The C atom shows a larger deviation than the H atom. Similar observations have been noticed in the literature (Scheins *et al.*, 2007; Jaradat *et al.*, 2007). For all aromatic C atoms of the *B* and *C* rings, which always carry a H atom, it has been observed that they have a higher volume than the other C atoms without hydrogen neighbours. All H atoms bonded to C atoms have volumes within the range 6.08–8.07 Å^3. The H atoms which are involved in intramolecular and intermolecular N—H···O hydrogen bonds have significantly smaller volumes between 2.7 and 3.6 Å^3 and higher positive charges of $\sim$ 0.3–0.4 e. This is in agreement with the Koch and Popelier criteria (Koch & Popelier, 1995).

6. Conclusions

The experimental densities of two chromone derivatives have been obtained by multipole refinement of high-resolution single-crystal X-ray diffraction data measured at a temperature of 100 K.

Our charge-density analysis has focused on a common O═C—C═C—N—H··· fragment in both chromone derivatives which may form a resonance-assisted hydrogen bond. A RAHB is accompanied by π-electron delocalization within the hydrogen-bonded ring containing a conjugated system of single and double bonds. A topological analysis revealed that the electron densities in the bond-critical points (BCPs) within the hydrogen-bonded ring are nearly the same in the two compounds. Values of the bond ellipticity in the ring are typical for double bonds. Application of the source function to the intramolecular hydrogen bond has confirmed the N—H···O hydrogen bond to be a resonance-assisted hydrogen bond. Both geometrical and topological parameters prove the π-character of bonds within the investigated O═C—C═C—N—H hydrogen-bonded ring. They also show that the intramolecular N—H···O hydrogen bonds are of medium strength, while other intermolecular C—H···O bonds are weak. According to Rozas's approach, which is based on the Laplacian of the electron density and the total energy density [$\nabla^2\rho(\mathbf{r}_{BCP})$ and $H(\mathbf{r}_{BCP})$] a partially covalent character can be assigned to both intramolecular hydrogen (N—H···O) bonds in (I) and (II), which is also reflected in the energy values of these hydrogen bonds. The analysis of atomic properties shows a strong similarity of both chromone derivatives, confirming the transferability of their electronic properties analogous to amino acids and peptides (Luger & Dittrich, 2007). Further studies of chromone derivatives are expected to give more information about the influence of the nearest and next-nearest neighbours within the hydrogen-bonded ring.

The high-resolution measurements were carried out within the projects I-20070020, I-20090042 EC at the light source DORIS III at HASYLAB/DESY, Hamburg, Germany. The research leading to these results has received funding from the European Community's Seventh Framework Programme (FP7/2007-2013) under grant agreement no. 226716. The authors thank the University of Łódź for financial support (University Research Grants – Grant No. 505/721/R 2010). The authors thank Professor E. Budzisz from Medical University of Lodz for supplying the crystals. Theoretical calculations have been carried out in the Cracow Supercomputing Centre (Poland).

References

Abramov, Yu. A. (1997). *Acta Cryst.* A**53**, 264–272.
Allen, F. H., Kennard, O., Watson, D. G., Brammer, L., Orpen, A. G. & Taylor, R. (1987). *Chem. Soc. Perkin Trans. 2*, pp. S1–83.
Allen, F. H., Kennard, O., Watson, D. G., Brammer, L., Orpen, A. G. & Taylor, R. (1992). *International Tables for X-ray Crystallography*, Vol. C, ch. 9.5, pp. 685–706. Amsterdam: Kluwer Academic Publishers.
Alkorta, I., Elguero, J., Mo, O., Yanez, M. & del Bene, J. E. (2004). *Mol. Phys.* **102**, 2563–2574.
Alkorta, I., Elguero, J., Mo, O., Yanez, M. & del Bene, J. E. (2005). *Chem. Phys. Lett.* **411**, 411–415.
Asmah Susidarti, R., Rahmani, M., Ismail, H. B. M., Sukari, M. A., Yun Hin, T.-Y., Ee Cheng Lian, G. & Manaf Ali, A. (2009). *Pharm. Biol.* **47**, 182–185.
Bach, A., Lentz, D. & Luger, P. (2001). *J. Phys. Chem. A*, **105**, 7405–7412.
Bader, R. F. W. (1990). *Atoms in Molecules. A Quantum Theory.* Oxford University Press.
Becke, A. D. (1993). *J. Chem. Phys.* **98**, 5648–5652.
Bernstein, J., Davis, R. E., Shimoni, L. & Chang, N.-L. (1995). *Angew. Chem. Int. Ed. Engl.* **34**, 1555–1573.
Bertolasi, V., Gilli, P., Ferretti, V. & Gilli, G. (1994). *Acta Cryst.* B**50**, 617–625.
Biegler-König, F. & Schonbohm, J. (2002). *J. Comput. Chem.* **23**, 1489–1494.
Budzisz, E., Brzezińska, E., Krajewska, U. & Różalski, M. (2003). *Eur. J. Med. Chem.* **38**, 597–603.
Budzisz, E., Graczyk-Wojciechowska, J., Zięba, R. & Nawrot, B. (2002). *J. New J. Chem.* **26**, 1799–1804.
Burnett, M. N. & Johnson, C. K. (1996). *ORTEP*III. Report ORNL-6895. Oak Ridge National Laboratory, Tennessee, USA.
Clementi, E. & Roetti, C. (1974). *At. Data Nucl. Data Tables*, **14**, 177–478.
Espinosa, E., Alkorta, I., Elguero, J. & Molins, E. (2002). *J. Chem. Phys.* **117**, 5529–5542.
Espinosa, E., Molins, E. & Lecomte, C. (1998). *Chem. Phys. Chem.* **285**, 170–173.
Etter, M. C. (1990). *Acc. Chem. Res.* **23**, 120–125.
Frisch, M. J. *et al.* (2003). *GAUSSIAN*03, Version 6.1. Gaussian Inc., Pittsburgh, PA, USA.
Gatti, C. & Bader, R. F. W. (1998). *Chem. Phys. Lett.* **287**, 233–238.
Gatti, C., Bianchi, R., Destro, R. & Merati, F. (1992). *J. Mol. Struct. Theochem*, **255**, 409–433.
Gatti, C., Cargnoni, F. & Bertini, L. (2003). *J. Comput. Chem.* **24**, 422–436.
Gilli, P., Bellucci, F., Ferretti, V. & Bertolasi, V. G. (1989). *J. Am. Chem. Soc.* **111**, 1023–1028.
Grabowski, S. J. (2003). *J. Phys. Org. Chem.* **16**, 797–802.
Grabowski, S. J. & Małecka, M. (2006). *J. Phys. Chem. A*, **110**, 11847–11854.
Grazul, M. & Budzisz, M. (2009). *Coord. Chem. Rev.* **253**, 2588–2598.

Hansen, N. K. & Coppens, P. (1978). *Acta Cryst.* A**34**, 909–921.
Jaradat, D. M. M., Mebs, S., Checinska, L. & Luger, P. (2007). *Carbohydr. Res.* **352**, 1480–1489.
Jeffrey, G. A. (1997). *An Introduction to Hydrogen Bonding.* Oxford University Press.
Jeffrey, G. A. & Saenger, W. (1991). *Hydrogen Bonding in Biological Structures.* Berlin: Springer-Verlag.
Johnas, S. K. J., Morgenroth, W. & Weckert, E. (2006). HASYLAB/DESY Annual Report, pp. 325–328. HASYLAB/DESY, Hamburg, Germany.
Kabsch, W. (1993). *J. Appl. Cryst.* **26**, 795–800.
Koch, U. & Popelier, P. L. A. (1995). *J. Phys. Chem.* **99**, 9747–9754.
Koritsanszky, T. S. & Coppens, P. (2001). *Chem. Rev.* **101**, 1583–1627.
Kostova, I. (2007). *Expert Opin. Drug Disc.* **2**, 1605–1618.
Kulkarni, M. V., Kulkarni, G. M., Lin, C.-H. & Sun, C.-M. (2006). *Curr. Med. Chem.* **13**, 2795–2818.
Luger, P. & Dittrich, B. (2007). *The Quantum Theory of Atoms in Molecules.* Weinheim: Wiley-VCH.
Madsen, A. Ø. (2006). *J. Appl. Cryst.* **39**, 757–758.
Madsen, G. K. H., Iversen, B. B., Larsen, F. K., Kapon, M., Reisner, G. M. & Herbstein, F. H. (1998). *J. Am. Chem Soc.* **120**, 10040–10045.
Małecka, M. (2007). *J. Mol. Struct.* **831**, 135–143.
Małecka, M. & Budzisz, E. (2006). *Acta Cryst.* E**62**, o5058–o5060.
Małecka, M., Grabowski, S. J. & Budzisz, E. (2004). *Chem. Phys.* **297**, 235–244.
Musa, M. A., Cooperwood, J. S. & Khan, M. O. F. (2008). *Curr. Med. Chem.* **15**, 2664–2679.
Ohemeng, K. A., Schweder, C. F., Fu, K. P. & Barret, J. F. (1993). *Bioorg. Med. Chem. Lett.* **3**, 225–230.
Overgaard, J. & Madsen, G. K. H. (2007). *D3_reduce*. HASYLAB. Department of Chemistry, University of Aarhus, Denmark.
Paulmann, C. (2006). *MarToolsCP*, Version 1.0. University of Hamburg, c/o HASYLAB/DESY, Germany.
Popelier, P. (2000). *Atoms in Molecules An Introduction.* Harlow, England: Pearson Education Limited.
Przybylski, P., Huczynski, A., Pyta, K., Brzezinski, B. & Bartl, F. (2009). *Curr. Org. Chem.* **13**, 124–148.
Rosskopt, F., Kraus, J. & Franz, G. (1992). *Pharmazie*, **47**, 139–142.
Rozas, I., Alkorta, I. & Elguero, J. (2000). *J. Am. Chem. Soc.* **122**, 11154–11161.
Rybarczyk-Pirek, A. J., Dubis, A. T., Grabowski, S. J. & Nawrot-Modranka, J. (2006). *Chem. Phys.* **320**, 247–258.
Rybarczyk-Pirek, A. J., Grabowski, S. J., Małecka, M. & Nawrot-Modranka, J. (2002). *J. Phys. Chem. A*, **106**, 11956–11962.
Scheins, S., Messerschmidt, M., Dittrich, B., Morgenroth, W., Paulman, C. & Luger, P. (2007). *J. Phys. Chem.* **111**, 5499–5508.
Sheldrick, G. M. (2008). *Acta Cryst.* A**64**, 112–122.
Volkov, A., Abramov, Y., Coppens, P. & Gatti, C. (2000). *Acta Cryst.* A**56**, 332–339.
Volkov, A., Macchi, P., Farrugia, L. J., Gatti, C., Mallinson, P., Richter, T. & Koritsanszky, T. (2006). *XD*2006. University at Buffalo, State University of New York, NY, USA; University of Milano, Italy; University of Glasgow, UK; CNRISTM, Milano, Italy; Middle Tennessee State University, TN, USA.